ELSEVIER

International Journal of Mass Spectrometry 215 (2002) 163–173

International Journal of Mass Spectrometry

www.elsevier.com/locate/ijms

Photoion imaging spectrometry in intense laser fields

Sarita Vig, M. Krishnamurthy, V. Kumarappan, D. Mathur*

Tata Institute of Fundamental Research, Homi Bhabha Road, Mumbai 400 005, India

Received 5 July 2001; accepted 5 November 2001

Abstract

We describe a photoion imaging spectrometer that makes use of a position sensitive detector (PSD) incorporating a delay-line anode system. We have used this spectrometer to probe the spatial alignment of molecules in moderately intense laser fields ($\sim 2 \times 10^{12}$ W cm^{-2}). The system is used to image the angular distributions as well as to probe the kinetic energy of ions formed in the process of ionization (fragmentation) of atoms (molecules) in intense laser fields. We have imaged Xe^+ in order to characterize the spatial and temporal properties of our spectrometer. The light-field-induced breakup of I_2 into $I^+ + I$ has also been imaged and the kinetic energy release determined for different laser polarization directions. We discuss the merits and limitations of delay line detector systems in imaging studies of molecular ionization and fragmentation in intense laser fields. (Int J Mass Spectrom 215 (2002) 163–173)

PACS: 33.80.Lg; 39.90.+d

Keywords: Position-sensitive detector; Time-of-flight; Momentum spectrometry; Intense laser fields; Field-induced molecular ionization

1. Introduction

Momentum spectroscopy has, in recent years, assumed a very important role in molecular dynamics experiments. It involves the determination of the momenta of fragment atoms or molecules that are produced in the course of an ionizing interaction involving either neutral molecules or molecular ions. The interaction may be either collisional or laser-induced. Detection of either electrons or ions or, preferably, a coincidence measurement of both, can provide valuable insights into kinematics and dynamics of molecular ionization and dissociation processes.

A simple time-of-flight mass spectrum can yield the momentum of an ion along the time-of-flight axis. An imaging spectrum alone would give the two components of momenta in the plane of the imaging detector. A major advance in momentum spectroscopy has recently been made with the technique christened "cold target recoil ion momentum spectroscopy" (COLTRIMS) [1] wherein the target gas in an ion–atom (molecule) collision setup is cooled by means of supersonic expansion before it interacts with the projectile ion beam. This has opened the possibility of measuring the very small values of momentum gained by recoil ions produced in the course of collisional ionization. A key to achieving the necessary high detection efficiencies, together with good momentum resolution in respect of recoil ions and electrons, is the deployment of a position sensitive detector (PSD). In order to obtain quantitative information on the total momentum vector of an ion produced in the course of the interaction, it becomes necessary to obtain, simultaneously, the ion's

* Corresponding author. E-mail: atmol1@tifr.res.in

1387-3806/02/$20.00
PII S1387-3806(01)00563-2

time-of-flight as well as the position at which it impinges on the detector. Although initial use of PSDs was mainly for atomic collision experiments (for a cogent review, see [2]), recently there have been attempts to integrate such detectors in apparatus used to study the interaction of atoms and molecules with strong laser fields [3,4].

Photoion spectroscopy with intense laser fields is an area of research that holds promise of new insights into non-perturbative molecular dynamics. In this context, the term "intense" implies laser intensities in excess of $10^{12}\,\mathrm{W\,cm^{-2}}$. At such intensities, the electric field generated within the focused laser spot becomes large in comparison to the Coulombic fields within atoms and molecules. Such laser-molecule interactions occur in a non-perturbative regime, and the atomic and molecular properties that drive the dynamics lie far from equilibrium. In interactions of molecules with such intense fields, studies to reveal sequential and non-sequential contributions to molecular multiple ionization [5] and correlated electron emission in multiphoton ionization [6] have led to better understanding of the physics governing the interaction of intense, transient electric fields with matter. Experiments involving measurements of fragment ion angular distributions [7], kinetic energy releases, and momentum distributions are now becoming feasible mainly because of developments in detector technology, particularly in respect of PSDs. A PSD of the kind discussed in this paper is capable of simultaneous measurement of three or four ions that may be formed in intense laser interaction. Such measurements would reveal otherwise inaccessible information, like the geometry of the molecular ion prior to fragmentation or the dynamics of multiple ionization and fragmentation pertaining to the questions like whether or not dissociation precedes multiple ionization.

In the present paper, we describe the development of a high mass-resolution photoion imaging spectrometer that is used to investigate processes involving the interaction of atoms and molecules with intense (10^{12} to $10^{16}\,\mathrm{W\,cm^{-2}}$) laser fields of picosecond or femtosecond duration. Ion imaging reveals information on the angular distributions of photoions formed in processes like ionization and dissociative ionization apart from quantitative insights into kinetic energy release processes that is obtained by measurement of ion arrival times. The measurement of ion angular distributions also provides the possibility of studying dynamics involved in the spatial alignment of molecules in intense laser fields [8,9].

In Section 2, we present the details of our spectrometer and, specifically, of the PSD system that we have incorporated into it. The calibration and characterization of the PSD system is described. In order to illustrate the efficacy of our spectrometer, we show how our imaging system is used to obtain the angular distributions of atomic ions like Xe^+ and fragment ions like I^+ that are produced upon field-induced photodissociation of I_2. The angular distribution of I^+ is explained in terms of the spatial alignment of the precursor I_2 molecule along the direction of laser polarization. We also discuss the applicability of the PSD system for studies in intense field ionization and discuss the merits and the limitations that a delay line anode system offers.

2. Position sensitive detector

Microchannel plate (MCP) assemblies along with anode systems are widely used for detecting single particles such as electrons, ions, and photons. A PSD comprises a microchannel plate assembly with an appropriate anode read-out system such that the determination of fragment ion impact position (imaging) and/or fragment ion time-of-flight (timing) with respect to an external trigger is possible.

A variety of anode systems may be used for the MCP read-out [10]. Phosphor screens combined with a CCD/video camera read-out have found utility as collecting anodes. The electron cloud produced when a particle impinges on the MCP is made to accelerate by a high voltage applied to the phosphor screen, and a CCD-frame grabber coupled to a computer images the luminescence produced on the screen. Such a system has obvious utility in direct determination of the position of particle impact. However, due to the usually

relatively slow electronic read-out of the optical image, it is not very useful for obtaining timing information. On the other hand, there are specially shaped anodes that give good electronic timing read-out but do not give any position information. Special segmented anodes combined with advanced electronic read-outs can also be used. Here, the charge collected on the different electrodes is collected and measured in order to obtain usually excellent position resolution and fair timing resolution. The charge integrating electronics is inherently slow, and the achievable count rate is quite limited compared to what the MCP itself is capable of. The most common amongst these kinds of anodes is the so-called wedge-and-strip anode system. Wester et al. [11] have adopted a novel method to determine the velocity distributions. The position information is obtained using a CCD-phosphor screen, and the timing information is deduced using thin anode strips placed in the path of the electrons before they impinge on the phosphor. The timing signals are then correlated to the positions of the corresponding ion impact recorded by the CCD using an independent transformation from the camera coordinates to the anode strips.

The PSD used by us is a delay line detector developed by Schmidt-Bocking and coworkers [10]. It consists of twin MCP plates (in chevron configuration), of 47 mm active diameter, with a delay line anode system used to detect charged particles. A schematic representation of the geometry of the detector system is shown in Fig. 1a. The anode system consists of a pair of helical wires, for each of the two spatial dimensions. The wires are wound on a ceramic frame. When the electron cloud from the MCP impinges on the wire, the signal pulses that reach both ends of the wire are detected, as shown schematically in Fig. 1b. The difference between the times taken by the signals

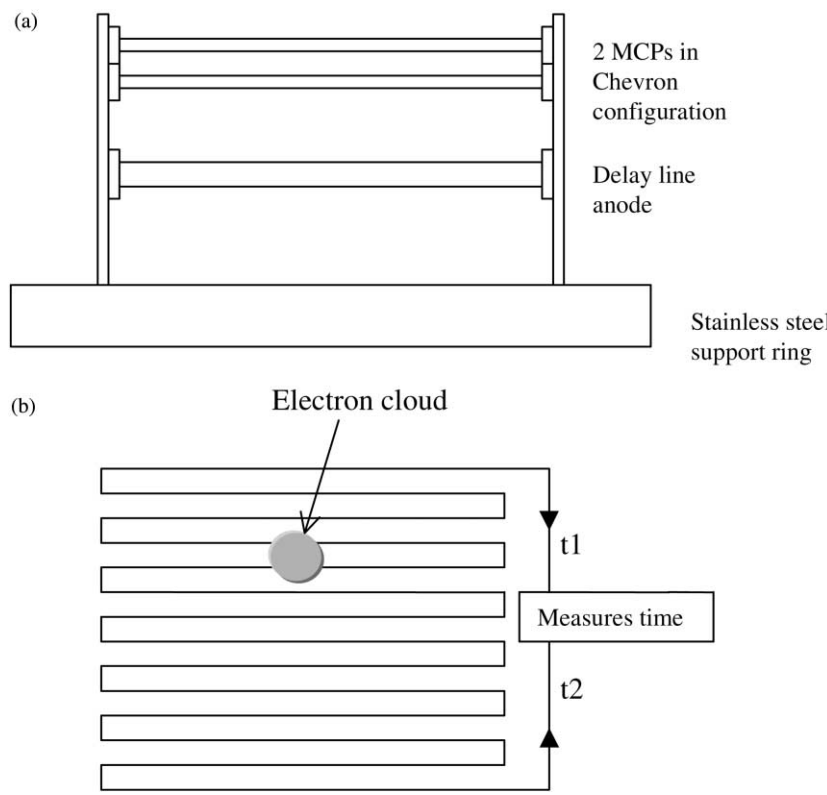

Fig. 1. (a) Schematic of the position sensitive detector system; (b) schematic of the delay line anode system.

to reach both the ends of the wire is proportional to the position of impact of the electron cloud. Since there are two such wire pairs wound perpendicular to each other on the ceramic frame, one can extract the two-dimensional position information about the incident charge cloud. The sum of the times taken by the signals to reach both ends of the wire in each dimension is constant, and can be used to determine the time taken by the charged particle to reach the detector. From this time-of-flight, information about the m/q ratio of the incident ions, as well as their kinetic energy, can be deduced. A pair of wires is used for each spatial dimension to eliminate any pickup and thus reduce the noise in the signal; a voltage difference of 20–40 V is applied between them.

The complete detector system consists of a 6-fold differential amplifier with constant fraction discriminator unit for every channel, a time-to-digital converter (TDC), along with the PSD. The electron cloud signal from the delay line is fed to the differential amplifier to eliminate noise pickup. The analog signals from the anode, after amplification, are fed to a suitably tuned constant fraction discriminator (CFD). These signals are then coupled to the TDC for time measurement and the data for each event is stored on the computer.

3. Calibration of the PSD

In order to test the capability of the detector for its position measurement, it is essential to calibrate the detector and determine the position resolution that is possible. Furthermore, it is also necessary to quantify other performance characteristics of the detector, such as detection uniformity and linearity in position. Initially, a defocused beam of electrons was allowed to impinge on the PSD, such that the total active area of the detector was uniformly exposed to electrons. From the uniform image obtained, it was possible to rule out the presence of any inactive spots on the microchannel plates. To determine spatial linearity of the PSD, a mask was made out of a 1 mm thick aluminium plate, with a large number of small, precise and uniformly-spaced holes. This mask was placed

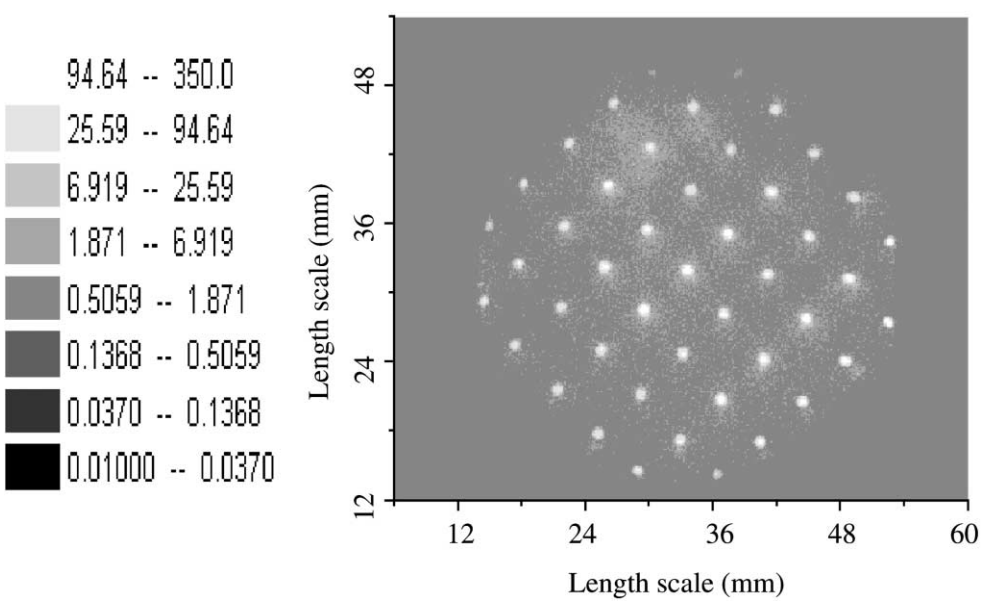

Fig. 2. Image obtained when a mask with precisely made holes is placed before the detector and irradiated with 300 eV electrons. The image indicates the absence of distortions on the detector. The length scale of 0.1 mm corresponds to 1 pixel.

directly in front of the detector, about a centimeter away from the channel plates. Uniform exposure of the mask to a flux of electrons (of 300 eV energy) produced an image of the type shown in Fig. 2; the uniformity of the image confirms the absence of image distortions.

In order to calibrate the PSD in terms of linearity and spatial resolution, a mask with varying sizes of holes and slits was placed before the detector. The holes and slits had precision diameters and openings that varied from 20 μm to 1 mm. By comparing the sizes of the holes and slits in the mask with those on the image obtained upon electron irradiation, a measure of the position resolution of the PSD can be obtained. Fig. 3a shows an image of the mask with varying sizes of apertures and holes. Fig. 3b shows the plot

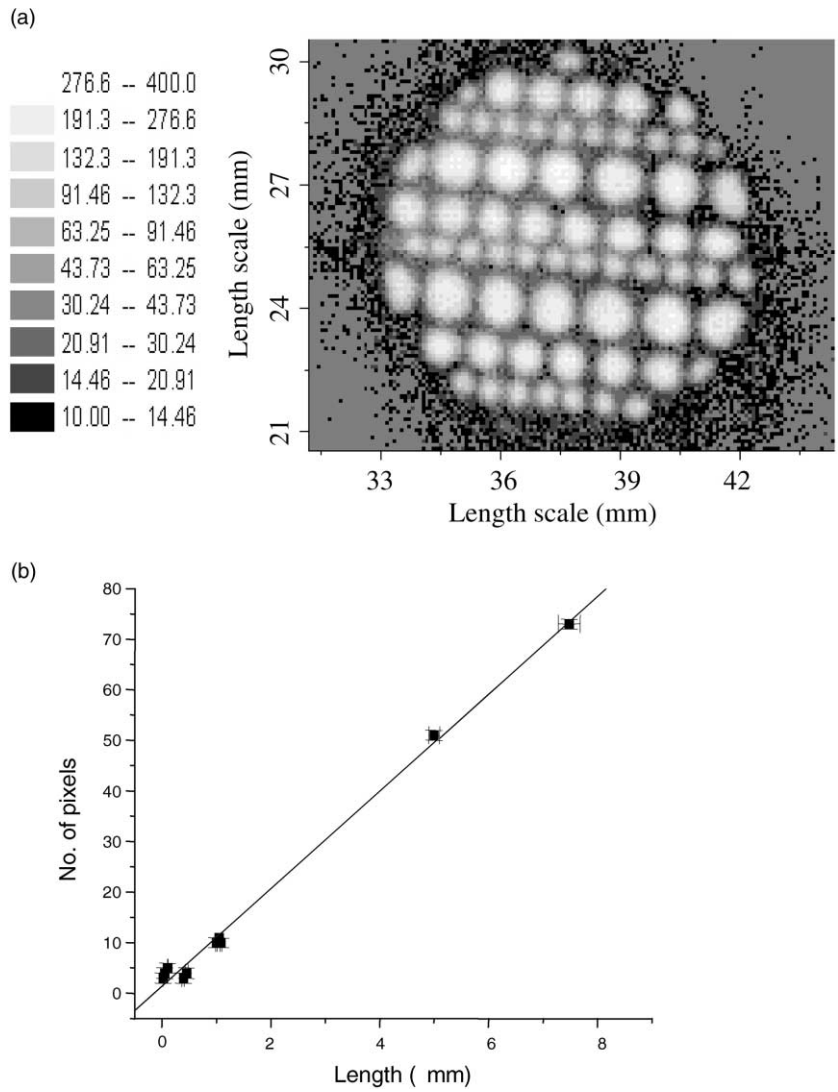

Fig. 3. (a) Image of the mask with varying sizes of apertures and holes obtained with 300 eV electrons; (b) the plot of the actual sizes (*x*-axis) vs. the number of pixels (*y*-axis) as obtained in the image. Slope gives the number of micrometers corresponding to 1 channel. Here, 1 channel ∼ 0.1 mm.

of the actual sizes (x-axis) vs. the number of pixels (y-axis) obtained in the image. The measured image correlates very well with the real sizes of holes and slits on the mask, as demonstrated by the linearity of the graph. The slope gives the number of pixels corresponding to 1 μm; in our case, this corresponds to ∼95 μm pixel^{-1}, which is very close to the value of 100 μm pixel^{-1} expected on the basis of data supplied by the manufacturers of the PSD.

4. Ion imaging

A schematic representation of the imaging spectrometer is shown in Fig. 4a. Our PSD has been incorporated into a two-field, time-of-flight mass spectrometer (TOFMS). Each of the three electrodes shown in the figure is 2 mm thick, with an inter-electrode spacing of 15 mm. A nickel wire mesh (70% transmission, 50 mm diameter) is placed at the center of the electrodes. The drift length in our TOFMS is 170 mm. Appropriate voltages are applied on the first two plates while the third plate, from which the drift region starts, is kept at ground potential. This ensures a field free drift region all the way up to detector. Another nickel wire mesh is also placed about 5 mm above the MCP, such that high voltage can be applied on the front plate of the MCP without causing any field penetration into the drift region. The base pressure of the chamber, in which the entire assembly is housed, is maintained at 10^{-9} Torr.

Laser pulses of 35 ps duration, wavelength 532 nm, and energy ∼2 mJ, are obtained from an Nd–YAG laser operating at 10 Hz repetition rate. It was ensured that the plane of polarization of the laser beam was kept parallel to the plane of the extraction electrodes of our TOFMS. The horizontally polarized laser beam was focused at the center of the extraction electrodes by means of a plano convex lens of 20 cm focal length. A fast photodiode collected scattered light from the laser and supplied the trigger pulse to the PSD. The electronics setup for the detector system is sketched schematically in Fig. 4b.

The sample gas of interest is introduced into the entire chamber through a needle valve such that the pressure rises to ∼2×10^{-8} Torr. The arrival time spectra of the ions extracted from the focal region is determined along with the position information. The data is recorded for each ion impinging on the detector. In our experiments, we collected data for a few thousand laser shots in order to carry out off-line analysis that yielded ion momentum images.

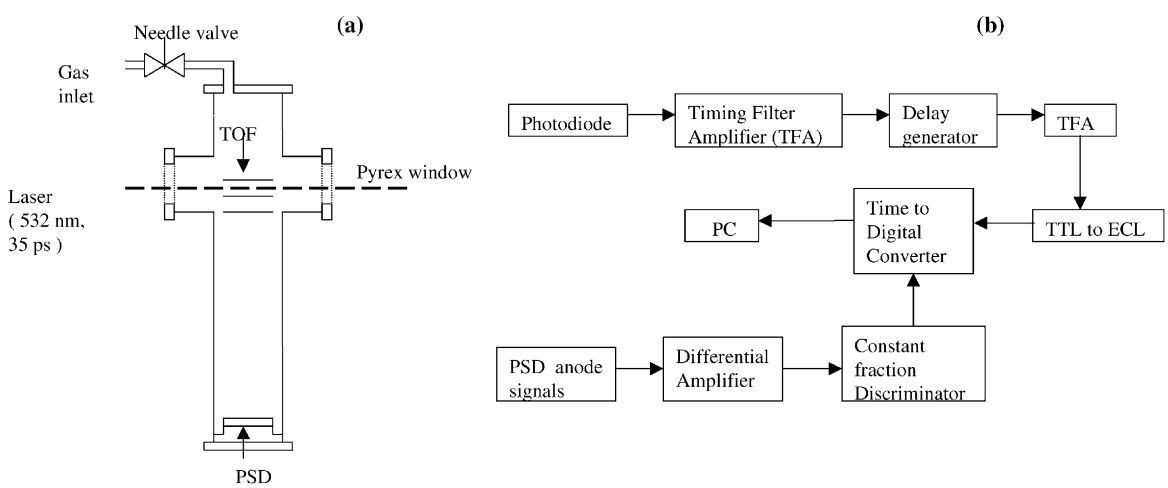

Fig. 4. (a) Schematic of the experimental setup with the time-of-flight mass spectrometer used for ion imaging; (b) schematic of the electronic setup for the detector system.

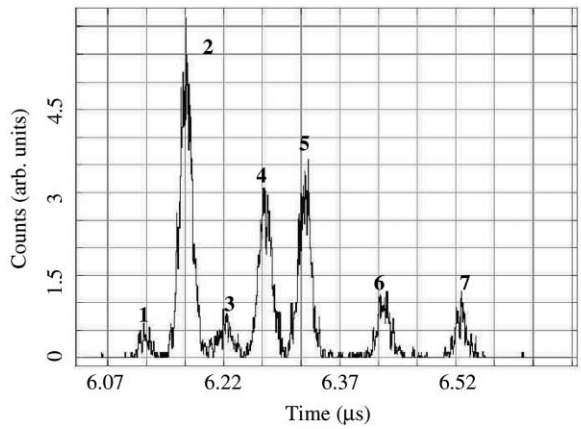

Peak	m/q	Natural abundance
1	127	1.9%
2	128	26.4%
3	129	4.1%
4	130	21.2%
5	131	26.9%
6	134	10.4%
7	135	8.9%

Fig. 5. Time-of-flight spectrum of xenon ions. The isotopes of xenon can be clearly distinguished but note that their relative abundances do not correspond to the natural abundances (see text).

5. Results and discussion

A typical time-of-flight spectrum of atomic Xe^+ ions is shown in Fig. 5. The major six naturally-occurring isotopes of Xe are clearly seen in this spectrum. The spectrum was obtained by placing the trigger to the PSD about 500 ns before the Xe^+ arrival time. This was necessary because our TDC can record only those ions that arrive within 6.5 μs after the trigger that, in our case, is a laser photodiode signal with an appropriate delay. Our data indicate that a time resolution of $\sim 2.5 \times 10^{-3}$ ($\Delta t/t$ of the peak corresponding to the $^{128}Xe^+$ ion) is obtained, giving an overall mass resolution ($\Delta m/m = 2 * \Delta t/t$) of 1/200 amu. We note that the measured isotope ratios do not correlate with the natural abundances. This is due to the fact that the PSD operates in a single-hit mode, with a frequency of 1 count μs^{-1}. Consequently, the probability of recording ions of successively higher values of m/q becomes progressively small and, hence the apparent distortion of relative abundance values depicted in Fig. 5.

A typical image of Xe^+ ions is shown in Fig. 6a. The image shows a circular spot, the size of which determines the momentum of the Xe^+ and should correspond to that associated with the thermal energy of the Xe atoms at room temperature. Moreover, the image spot, as is expected, remains the same irrespective of the direction of laser polarization. The number of pixels corresponding to Xe^+ was measured to be 16. We have carried out ion trajectory calculations in order to correlate the experimental data with the position map for our TOFMS geometry and operating conditions. In our simulations, isotropically distributed Xe^+ ions with thermal energy were made to reach the detector and the position of arrival on the detector for different azimuthal and elevation angles was determined. Fig. 6b shows the computed image. A circular image of 18 pixels width is obtained and corresponds well with the experimental data. The measured value of time-of-flight is also the same as that obtained in simulations, to within 100 ns.

Fig. 7a and b show typical images of I^+ fragments produced upon dissociative ionization of I_2 into $I+I^+$. We have made these measurements at laser intensities that are below the threshold for the $I^+ + I^+$ channel, which results from double ionization of I_2 to $I_2{}^{2+}$. The intensity is kept low by introducing neutral density filters in the path of the laser beam. It is clear from the image that the angular distribution of I^+ ions in Fig. 7a is distinctly different from that of Xe^+ ions. Two lobes are distinctly observed in the former case, indicating an anisotropic angular distribution. The lobes

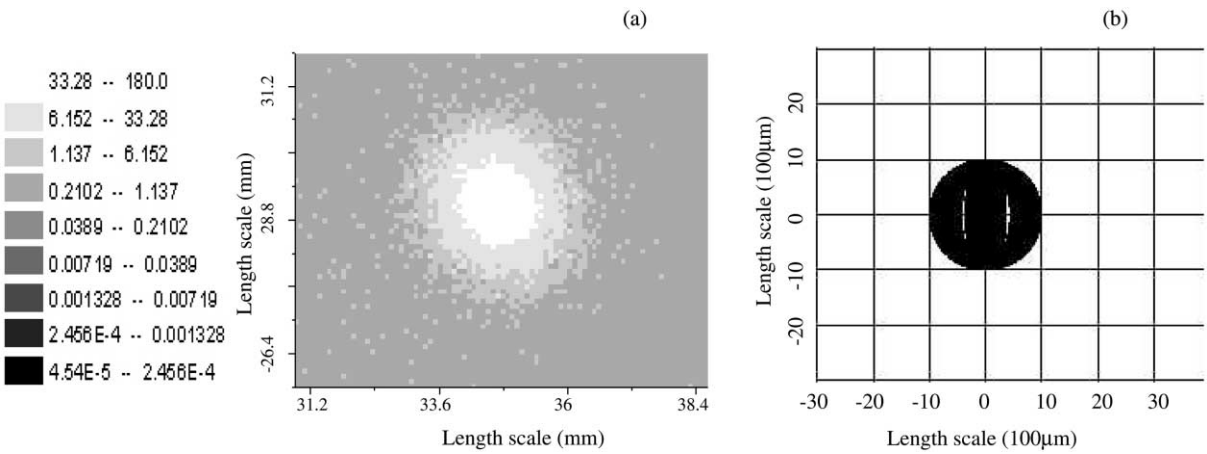

Fig. 6. (a) Image of thermal-energy Xe^+; (b) simulated image of Xe^+ ions possessing a thermal energy distribution.

indicate that the probability of detecting I^+ ions along the direction of laser polarization is maximum, and it is minimum in the direction that is perpendicular to the laser polarization vector. This is because the majority of I^+ ions formed due to interaction with intense laser field are due to I_2 molecules that become spatially aligned along the direction of laser polarization. Laser-field-induced fragmentation of aligned I_2 molecules results in formation of I^+ fragments whose initial momenta are such that the fragment ions follow a parabolic path towards the detector in the presence of the extraction field of the TOFMS. The larger the initial momentum that is imparted, the farther they would move from the center, with a corresponding inter-lobe separation manifesting itself in our detector image. The angular distribution seen in our image correlates well with previous measurements [12,17]. The radial distribution can be used to obtain the kinetic energy release in the fragmentation process while the angular distributions yield information on the extent of spatial alignment, or on the angle-dependent ionization probability [13].

On the other hand, when the laser polarization is made vertical, i.e., it is parallel to the direction of the extraction electric field of the TOFMS, the I^+ image that we obtained was a circular, isotropic spot (Fig. 7b). This can be attributed to the fact that since the laser polarization is along the TOF axis, I_2 molecules tend to align along that direction. Consequently, the fragmented I^+ ions would follow a straight trajectory to the PSD, leading to the isotropic distribution. However, those I^+ fragments that initially move in a direction away from the detector are decelerated until they stop and subsequently reverse their motion towards the PSD. The motion of such ions is identical to the I^+ fragments that initially accelerated towards the detector, except that they are delayed by a time that is equal to their turn-around time, which is twice the deceleration time. If the kinetic energy released upon dissociation of the I–I bond is large enough, the time difference between the forward and backward moving ions results in two well resolved peaks. The resulting temporal separation enables us to deduce a value of 0.8 eV for the most probable kinetic energy of an I^+ fragment. Our value correlates well with the kinetic energy release values measured by Laberge et al. (0.7 eV) [14] and more recent experiments conducted by Rosca-Pruna et al. [17] (0.87 eV) for each fragment in the (1, 0) channel of $I_2{}^+$ at 800 nm for a pulse duration of 3.9 ps. It is of interest to note that Normand and Schmidt [15] have reported a value of 0.6 eV for the *total* dissociation energy with 100 fs infrared pulses. This latter value also correlates with a report of Gibson et al. [16] where a total KER value of 0.7 eV is deduced for the $I + I^+$ channel.

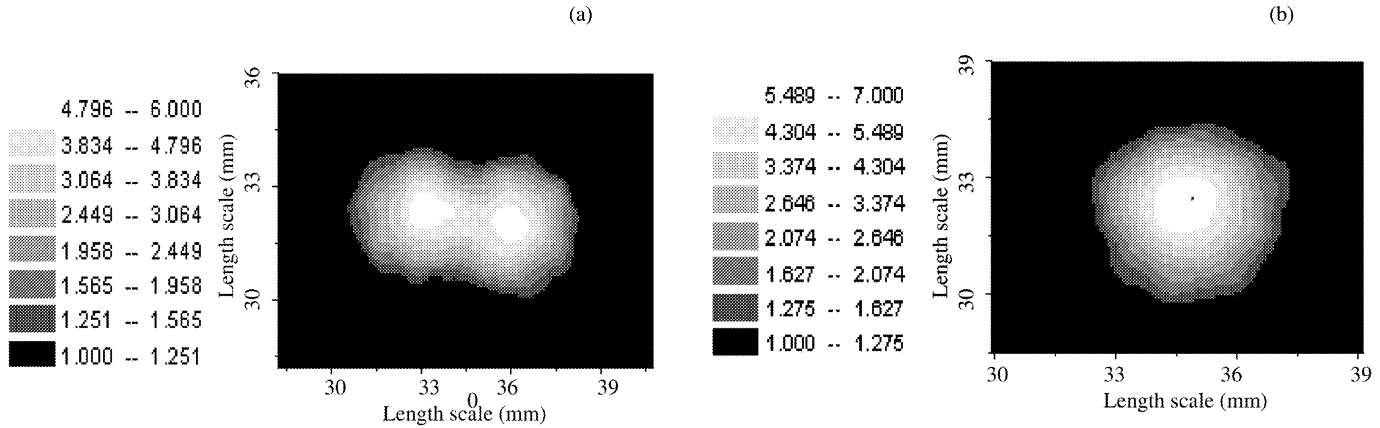

Fig. 7. (a) Image of the angular distribution of I^+ ions obtained from the $I + I^+$ channel when the laser polarization is perpendicular to the extraction field of the TOFMS. The lobe structure indicates the alignment of the I_2 molecule in the plane of the detector; (b) image of the angular distribution of the I^+ ions obtained from the $I + I^+$ channel when the laser polarization is parallel to the extraction field of the TOFMS. The isotropic distribution indicates the alignment of the I_2 molecule perpendicular to the plane of the detector.

6. Merits and limitations

A delay line anode system is, in principle, a most powerful imaging method. Its strength lies in the fact that position measurements can be made with very good spatial resolution while temporal resolution is not compromised. With multi-hit capability, this opens up the possibility of determining the momentum of three or four fragment ions that may be simultaneously formed in a molecular ionization event. This detector is also capable of handling a particle detection rate of ∼1 MHz (or an average of a particle in ∼1 μs). These advantages have recently been fully utilized in studies of the collisional ionization of atoms [1].

However, this may not be the best-suited system for ionization studies using intense laser beams. In such studies, while the average count rate may be relatively small, instantaneous count rates can be very large. If two particles simultaneously impinge on the detector, the ability to decipher the position simultaneously with a delay line system has limitations. Undistorted ion images are obtained only when the ion count rate is kept below 0.1 counts per laser shot. We have found that upon increasing the laser intensity, the two lobes of our I^+ ion image becomes distorted into a single spherical profile. Space charge effects can be ruled out as a potential cause of such distortion because these would enlarge the lobes rather than constrict them.

We illustrate this limitation by presenting, in Fig. 8, a momentum map of I^+ (produced in the $I + I^+$ channel) determined in the present experiments. P_y is the component of momentum along the direction of propagation of the laser beam while P_x depicts the momentum component perpendicular to the extraction field of the TOFMS. The momentum image can be used to deduce a value for the kinetic energy release. However, the value that we obtain does not correlate with that determined from simple time-of-flight mass spectra. For a value of 0.8 eV obtained from simple TOF spectrometry, we expect the momentum distribution to peak at $P_x \sim 116$ a.u. However, the image that is obtained shows the peak at $P_x \sim 28$ a.u., a value that is approximately four times smaller. We attribute this to the following. As the count rate increases, the I^+ image constricts, towards the center of the two lobes. This results in a smaller value for the measurement of the radial position and, hence, a correspondingly smaller value is deduced for the momentum.

This illustrates the serious limitation of delay line systems in application in intense-field-induced

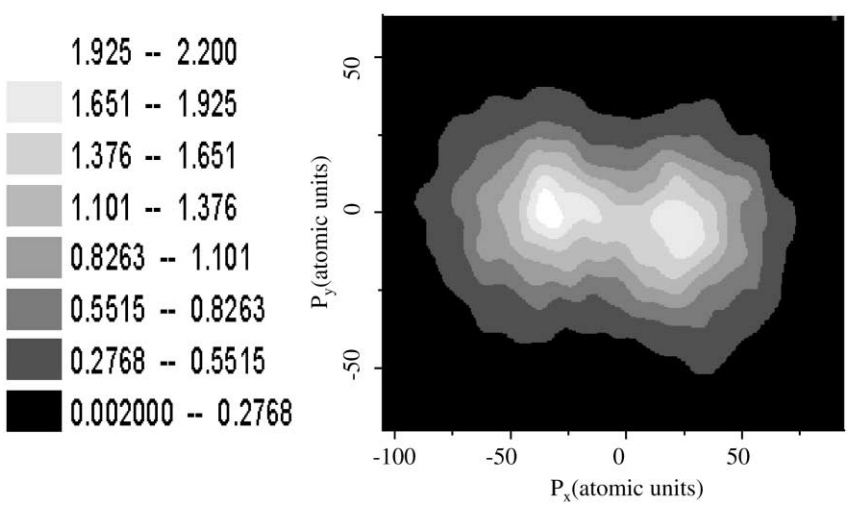

Fig. 8. Momentum map of I^+ ions when laser polarization is perpendicular to the extraction field of the TOFMS. P_y is the component of momentum along the laser propagation direction and P_x is the component of momentum along the polarization direction.

multiple ionization studies. Laser intensities in excess of 10^{14} W cm^{-2} are usually required to produce multiple charged fragment ions in case of simple molecules like N_2, CO, etc. At such intensities, laser focal volume effects become very important [18,19]. At such intensities, the count rate of the singly-charged parent ion in the laser focal volume far exceeds the count rates that can be handled by the detector. Consequently, momentum measurements are hampered. For example, consider the $I^+ + I^+$ channel. When the laser intensity in increased in order to observe this channel, the focal volume that has intensity to induce $I^+ + I$ channel is large enough that the count rate of I^+ from these events dominate and induce distortions in the image. Another example of this limitation is as follows: say one is interested in measuring simultaneous detection of C^+ and S^+ from dissociative ionization of CS_2. The threshold intensity for C^+ production far exceeds that of S^+. In such a case, when the intensity to produce C^+ is reached, the S^+ count rate is already large enough to induce gross distortions in position measurement.

Acknowledgements

We thank Dr. Shiromaru and F.A. Rajgara for their help in setting up the detector and Dr. Ullmann-Pfleger and Dr. O. Jagutzki for their help in using the detector.

References

[1] V. Mergel, R. Dorner, J. Ullrich, O. Jagutzki, S. Lencinas, S. Nuttgens, L. Spielberger, M. Unverzagt, C.L. Cocke, R.E. Olson, M. Schulz, U. Buck, H. Schmidt-Bocking, Nucl. Inst. Methods B 98 (1995) 593.
[2] J. Ullrich, R. Moshammer, R. Dorner, O. Jagutzki, V. Mergel, H. Schmid-Bocking, L. Spielberger, J. Phys. B 30 (1997) 2917.
[3] R. Dorner, H. Brauning, J.M. Feagin, V. Mergel, O. Jagutzki, L. Spielberger, T. Vogt, H. Khemliche, M.H. Prior, J. Ullrich, C.L. Cocke, H. Schmidt-Bocking, Phys. Rev. A 57 (1998) 1074.
[4] Th. Weber, M. Weckenbrock, A. Staudte, L. Spielberger, O. Jagutzki, V. Mergel, F. Afanch, G. Urbasch, M. Vollmer, H. Giessen, R. Dorner, Phys. Rev. Lett. 84 (2000) 443.
[5] Th. Weber, M. Weckenbrock, A. Staudte, L. Spielberger, O. Jagutzki, V. Mergel, F. Afaneh, G. Urbasch, M. Vollmer, H. Giessen, R. Dörner, J. Phys. B 33 (2000) L127.
[6] Th. Weber, H. Giessien, M. Weckenbrock, G. Urbasch, A. Staudte, L. Spielberger, O. Jagutzki, V. Mergel, M. Vollmer, R. Dorner, Nature 405 (2000) 658.
[7] A.S. Bracker, E.R. Wouters, A.G. Suits, Y.T. Lee, O.S. Vasyutinskii, Phys. Rev. Lett. 80 (1998) 1626.
[8] G. Ravindra Kumar, P. Gross, C.P. Safvan, F.A. Rajgara, D. Mathur, Phys. Rev. A 53 (1996) 3098.
[9] S. Banerjee, D. Mathur, G. Ravindra Kumar, Phys. Rev. A 63 (2001) 045401.
[10] R. Dorner, V. Mergel, O. Jagutzki, L. Spielberger, J. Ullrich, R. Moshanmer, H. Schmidt-Bocking, Phys. Reports 330 (2000) 95.
[11] R. Wester, F. Albrecht, M. Grieser, L. Knoll, R. Repnow, D. Schwalm, A. Wolf, A. Baer, J. Levin, Z. Vager, D. Zajfman, Nucl. Instrum. Methods A 413 (1998) 379.
[12] J.J. Larsen, N.J. Morkbak, J. Olesen, N. Bjerre, M. Machholm, S.R. Kelding, H. Stapelfeldt, J. Chem. Phys. 109 (1998) 8857.
[13] S. Banerjee, G. Ravindra Kumar, D. Mathur, Phys. Rev. A 60 (1999) R3369.
[14] M. Laberge, P. Dietrich, P.B. Corkum, in: J.L. Martin, A. Migus, G.A. Mourou, A.H. Zewail (Eds.), Ultrafast Phenomena VIII, Springer, Berlin, 1993.
[15] D. Normand, M. Schmidt, Phys. Rev. A 53 (1996) R1958.
[16] G.N. Gibson, M. Li, C. Guo, J.P. Nibarger, Phys. Rev. A 58 (1998) 4723.
[17] F. Rosca-Pruna, E. Springate, H.L. Offerhaus, M. Krishnamurthy, C. Nicole, M.J.J. Vrakking, J. Phys. B, submitted for publication.
[18] S. Banerjee, G. Ravindra Kumar, D. Mathur, J. Phys. B 32 (1999) L305.
[19] S. Banerjee, G. Ravindra Kumar, D. Mathur, J. Phys. B 32 (1999) 4277.